CrystEngComm

RSC Publishing

PAPER

View Article Online
View Journal | View Issue

Published on 06 September 2013. Downloaded by Universidad de Granada on 02/12/2013 06:34:40.

Cite this: *CrystEngComm*, 2013, **15**, 9968

Influence of chemical and structural factors on the calcite–calcium oxalate transformation

E. Ruiz-Agudo,*[ab] P. Álvarez-Lloret,[bc] C. V. Putnis,[a] A. B. Rodriguez-Navarro[b] and A. Putnis[a]

Received 1st July 2013,
Accepted 6th September 2013

DOI: 10.1039/c3ce41294f

www.rsc.org/crystengcomm

The mechanisms and epitaxial relationships of the replacement of calcite by calcium oxalate have been studied by means of SEM, 2D-XRD and AFM techniques. At acidic pH, oxalate-bearing solutions react with freshly cleaved calcite fragments through a pseudomorphic, coupled dissolution–precipitation reaction. This replacement reaction takes place by the dissolution of the calcite substrate followed by the precipitation of whewellite ($CaC_2O_4{\cdot}H_2O$) crystals, which nucleate and grow epitaxially on the (104) calcite surface. There are two sets of preferred orientations of the whewellite crystals (COM) on the calcite surface (Cc): $(010)_{COM}\|(104)_{Cc}$, $[100]_{COM}\|[\bar{4}41]_{Cc}$, and $(100)_{COM}\|(104)_{Cc}$, $[001]_{COM}\|[010]_{Cc}$. These epitaxial relationships can be understood when comparing the crystalline structure of both minerals. Simultaneous evolution of porosity in this system indicates that solute transport at the mineral–fluid interface is the rate-limiting step necessary to achieve spatial coupling between calcite dissolution and calcium oxalate nucleation and growth so that a pseudomorph is obtained. Understanding the mechanisms that control these mineral reactions has far-reaching implications for the understanding of many processes including the design of protective treatments for building stones or the optimization of phosphorus availability in soils. The results of this study may also offer interesting insights into the mechanisms of stone formation in the presence of biological fluids.

Introduction

Mineral replacement reactions play a very important role in many natural processes. Particularly, the transformation of calcium carbonate into calcium oxalate is critical in the control of processes as varied as Ca-oxalate stone formation in body fluids, the development of protective patinas on calcitic building stones (such as marble and limestone) or nutrient availability in calcareous soils. In these processes, there is a pre-existing mineral (*i.e.* calcite) that is replaced by Ca-oxalate and that induces its crystallization by heterogeneous nucleation.[1,2] These processes are facilitated if there is a structural similarity, that is, epitaxy, between the two mineral phases.

Despite the ubiquity and importance of processes involving the transformation of Ca-oxalate from calcite, the exact mechanism of this transformation on a nanoscale remains essentially unexplored. Experimental observations suggest that the growth of oxalates on calcite follows the typical pattern of a replacement (*i.e.* dissolution–reprecipitation) reaction where the parent calcite phase acts as a template for nucleation of the new phase.[1] Geider and co-workers[1] suggested that calcium oxalate grows epitaxially on calcite on the basis of lattice fit calculations and the observation of the regular orientation of oxalate crystals on calcite crystals, but no experimental evidence of the epitaxial relationship between the parent crystal and the overgrowth has been given. Also, it is critical to study how the texture and porosity change during the replacement reaction and which factors control them, since these properties ultimately determine the progress of the replacement reaction.[3–6]

The lack of sound mechanistic knowledge of the $CaCO_3$–CaC_2O_4 transformation has limited the development of effective treatments to control or prevent this transformation, for instance, during stone formation in biological fluids, in the design of conservation protocols for calcitic building stones or in the development of procedures for increasing the availability of plant nutrients (phosphorous) in soils. It is therefore the aim of this work to investigate the mechanism of the replacement of calcite by calcium oxalate, including the possible epitaxial relationships between the substrate and the product. This has been done by a combination of Scanning Electron Microscopy (SEM), bidimensional X-Ray Diffraction (2D-XRD) and Atomic Force Microscopy (AFM) techniques. Also, the effects of pH, oxalate concentrations, and fluid-to-solid ratio on this transformation have been evaluated.

[a] *Institut für Mineralogie, Universität Münster, Corrensstrasse 24, Münster, 48149, Germany. E-mail: encaruiz@ugr.es*
[b] *Department of Mineralogy and Petrology, University of Granada, Fuentenueva s/n, Granada, 18002, Spain*
[c] *Departmento de Geología, Universidad de Oviedo, c/ Jesús Arias de Velasco s/n, 33005, Oviedo, Spain*

This journal is © The Royal Society of Chemistry 2013

Published on 06 September 2013. Downloaded by Universidad de Granada on 02/12/2013 06:34:40.

Materials and methods

(a) Replacement reactions in Teflon® reactors

Replacement experiments were performed at room temperature (23 ± 1 °C) in sealed Teflon® reactors, with internal volumes of 65 and 250 mL. The temperature and pH of the experiments were selected so that the validity of our results extends to a wider range of applications including the design of protective coatings for calcitic building stones (*e.g.*, marble or limestone) or increase of nutrient availability in calcareous soils. Small cleavage fragments (0.030 ± 0.005 mg weight, *ca.* 4 × 3 × 1 mm in size) of optical quality calcite single crystals (Iceland spar) were weighed and placed into the reactors before 60 mL and 200 mL (depending on the volume of the reactor) of reaction solutions were added. After the reaction, the reactors were opened and the solids were rinsed with ethanol and dried overnight at 60 °C. Experiments were performed at acidic pH (3) starting from an aqueous solution of oxalic acid at concentrations of 0.1, 1, 10 and 100 mM and different reaction times (see Table 1 for a summary of the experimental conditions). Acidic conditions are locally expected in monuments or calcareous soils where oxalic acid (among other organic acids) is segregated by living organisms such as cyanobacteria or fungi. Some additional experiments were also performed at pH close to neutrality (6.5); pH was adjusted by the addition of HCl or NaOH. We selected this additional pH taking into account that the physiological pH range is 4.8 to 8.0, and at pH 6.5 and under normal Ca concentrations in urine, calcium oxalate is the main mineral formed.[7]

(b) Textural and two-dimensional X-ray diffraction analysis of reacted solids

A JEOL 6300F Field Emission Scanning Electron Microscope (FESEM) was used for morphology and texture examinations at different contact times between the calcite fragments and the oxalate-bearing solutions. To examine the surface morphologies of the samples after the replacement reaction, solids were carbon coated and secondary electron images were acquired by FESEM. For textural investigations, partially replaced crystals of selected samples were embedded into epoxy resin blocks and polished. Those samples were then carbon coated and examined by FESEM in backscattered electron mode. The observations were carried out at an accelerating voltage of 3 kV. Contrast in a backscattered image is given by the average molecular weight of the different phases present. Together with the differences in texture, this allows discriminating between the parent crystal and the replacement product.

2D-XRD analyses were performed to establish the crystallographic relationships between calcite and Ca-oxalate overgrowths using an X-ray single-crystal diffractometer equipped with a CCD area detector (D8 SMART APEX, Bruker, Germany). For the diffraction experiments, the working conditions were Mo Kα (λ = 0.7093 Å), 50 kV, and 30 mA, a pin-hole collimator of 0.5 mm in diameter, and an exposure time of 20 s per frame. Samples were measured using reflection mode. The ω and 2θ angles were set at 10 and 20°, respectively, and the sample was rotated around the Φ angle (a frame was registered every 5 degrees). The 2θ scan profiles were obtained by radial integration of the Debye–Scherrer rings that appeared on the bidimensional X-ray diffraction patterns, and pole densities/figures for the main calcite and whewellite reflections were calculated from the registered frames using XRD2DScan software.[8] These pole figures represent the variation in diffraction intensity of a given (*hkl*) plane with respect to the orientation of the specimen. If one or several intensity maxima are observed in specific areas of the pole figure, the sample shows a preferred orientation. The morphology of the calcium oxalate crystals as well as the crystallographic relationships found was simulated using SHAPE software.

(c) *In situ* Atomic Force Microscopy (AFM) observations

Experiments were carried out at 23 ± 1 °C *in situ* in a fluid cell of a Digital Instruments (Bruker) Multimode AFM working in contact mode. AFM images were taken by scanning a conical Si_3N_4 tip (spring constant, 0.12 N m^{-1}) attached to a 200 μm cantilever (Bruker). Sometimes, shorter tips (100 μm) with a spring constant of 0.48 N m^{-1} were used. Freshly cleaved, optically clear (104) calcite (Iceland spar from Mexico) surfaces were used as substrates.

AFM observations were performed starting from a solution slightly supersaturated with respect to whewellite (saturation index, SI = 0.17) and highly undersaturated with respect to calcite. The saturation index is defined as

$$\mathrm{SI} = \log \Omega = \log \frac{\mathrm{IAP}}{K_{\mathrm{sp}}} = \log \frac{a_{\mathrm{Ca}^{2+}} \cdot a_{\mathrm{anion}}}{K_{\mathrm{sp}}} \quad (1)$$

where Ω is the supersaturation, IAP is the ion activity product, $a_{\mathrm{Ca}^{2+}}$ is the calcium activity in solution, a_{anion} is the carbonate or oxalate activity in solution (for calcite or calcium oxalate, respectively) and K_{sp} is the solubility product of the phase considered. Despite being initially supersaturated with respect to both whewellite ($CaC_2O_4 \cdot H_2O$) and weddellite ($CaC_2O_4 \cdot 2H_2O$), no spontaneous precipitation was detected by visual inspection during solution preparation or in subsequent hours. The pH was fixed to 6.5 ± 0.1, and in this way,

Table 1 Summary of the experimental conditions in batch reaction experiments

Experiment	[Ox] (mM)	pH	Reaction time (h)	Solution volume
OX001	0.1	3.0	72	60
OX002	1.0	3.0	72	60
OX003	10.0	3.0	72	60
OX004	100.0	3.0	72	60
OX005	0.1	6.5	72	60
OX006	1.0	6.5	72	60
OX007	10.0	6.5	72	60
OX008	100.0	6.5	72	60
OX009	1	3.0	72	60
OX010	1	3.0	120	60
OX011	1	3.0	168	60
OX012	1	3.0	168	200

Published on 06 September 2013. Downloaded by Universidad de Granada on 02/12/2013 06:34:40.

the release of calcium from the calcite surface takes place at a much slower rate, allowing a more precise control of the nucleation and growth rate of the oxalate phase.

(d) Modelling of the evolution of solution composition

Activities of different chemical species and supersaturation with respect to possible phases in the system were calculated using PHREEQC.[9] The values of the solubility products of calcium oxalate phases and association constants in solution were not available in the used database, so the data found in the literature (Table 2) were introduced in the model of the aqueous phase composition. PHREEQC calculations enable ultimately the simulation of the evolution of the solution composition during the replacement reaction and the estimation of the amounts of dissolved calcite and precipitated whewellite during the course of the replacement.

Table 2 Values of solubility products of calcium oxalate phases and association constants used in PHREEQC[8] calculations

	Association constant[a] ($\log k$)
$HC_2O_4^- + H^+ = H_2C_2O_4$	4.266
$C_2O_4^{2-} + H^+ = HC_2O_4^-$	1.252
$C_2O_4^{2-} + Ca^{2+} = CaC_2O_4$	3.187
$C_2O_4^{2-} + Na^+ = NaC_2O_4^-$	1.035
	Solubility product[a] ($\log k_{sp}$)
COM	−8.69
COD	−8.43
COT	−8.28

[a] Values taken from Brecevic *et al.*[10]

Results

(a) Microscopic features of partially reacted crystals

SEM examinations of surfaces and cross-sections of reacted samples show that calcite is replaced pseudomorphically by calcium oxalate monohydrate (whewellite, based on X-ray diffraction analyses) according to two contrasting replacement textures, which were very sensitive to the pH of the starting solution. In both cases, the replacement product is polycrystalline. At pH 3, calcite fragments were completely covered by whewellite crystals after 24 h of contact with 1 mM oxalate solution. Fig. 1a shows the typical morphologies of the newly formed $CaC_2O_4{\cdot}H_2O$ crystals growing on the calcite surface. The crystal habit of the overgrowing whewellite is predominantly tabular with {010} forms bounded by {100} side faces (Fig. 1e). They appear clearly oriented on the calcite substrate,

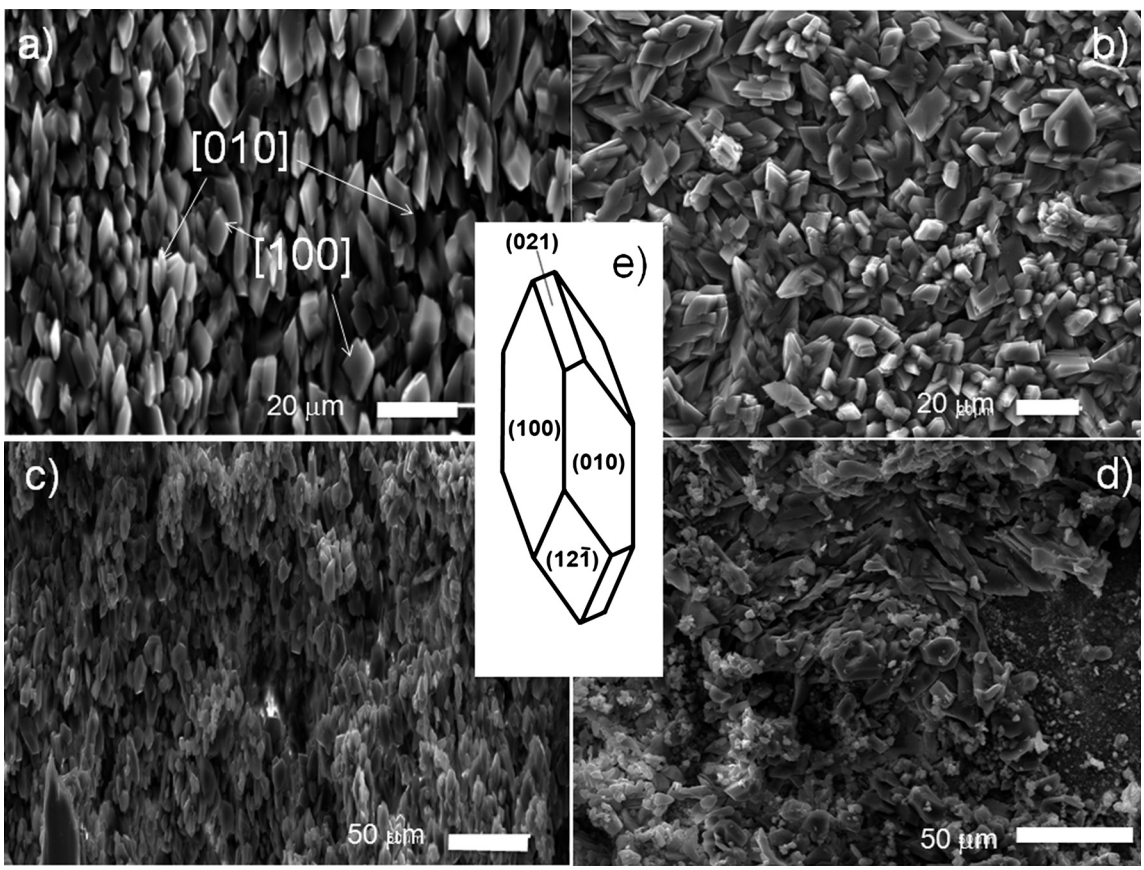

Fig. 1 FESEM secondary electron images of calcite crystals partially replaced by Ca-oxalate. Surfaces of partially replaced crystals after 72 hours of contact with (a) 1 mM oxalate solution, pH 3.0, solution volume, 60 mL; (b) 0.1 mM oxalate solution, pH 3, solution volume, 60 mL; (c) 10 mM oxalate solution, pH 3.0, solution volume, 60 mL; and (d) 100 mM oxalate solution, pH 3, solution volume, 60 mL. (e) Simulation of whewellite morphology using SHAPE, based on the FESEM observations.

 This journal is © The Royal Society of Chemistry 2013

Published on 06 September 2013. Downloaded by Universidad de Granada on 02/12/2013 06:34:40.

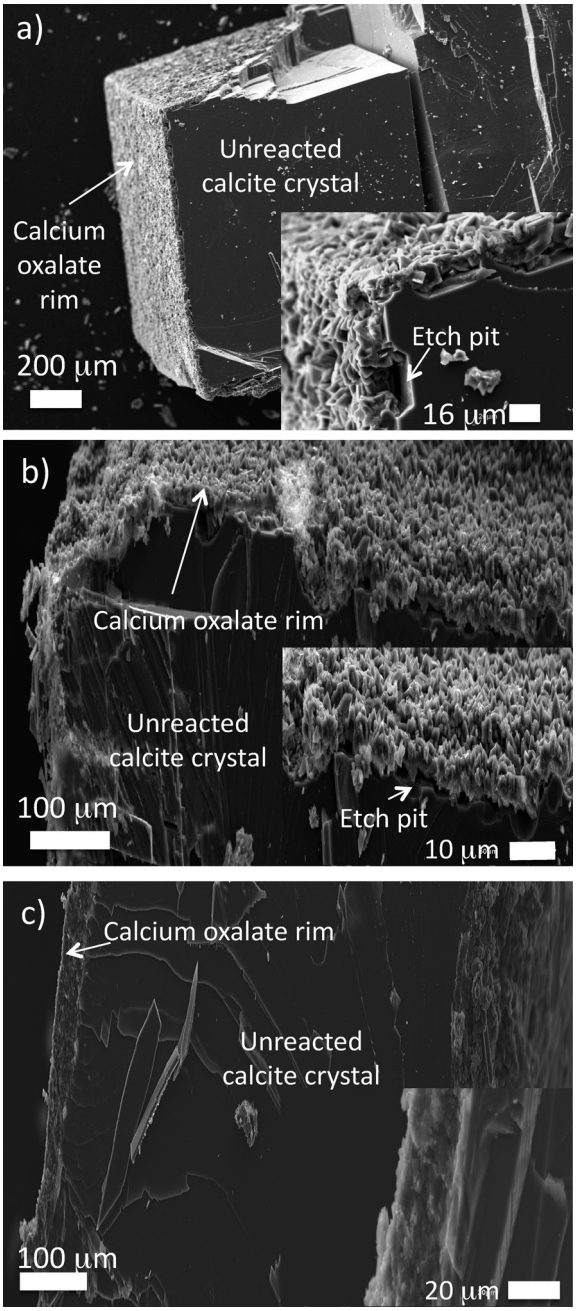

Fig. 2 FESEM secondary electron images of calcite crystals partially replaced by Ca-oxalate. Cross-section of a partially replaced crystal after 72 hours of contact with (a) 0.1 mM oxalate solution (pH 3.0, solution volume, 60 mL), (b) 1 mM oxalate solution (pH 3.0, solution volume, 60 mL), (c) 100 mM oxalate solution (pH 3.0, solution volume, 60 mL). Details of the sections are shown in the insets. Etch pits formed in the substrates are marked by arrows.

forming a thick layer on the calcite surface (Fig. 1a and 2b). However, at lower oxalate concentrations (0.1 mM, Fig. 1b) and acidic pH (3), whewellite crystals appear to be randomly distributed on the calcite surface. A gap is observed between the reaction product and the calcite substrate for concentrations below 10 mM. Whether this is a consequence of the sample preparation protocol or a consequence of the reaction cannot be unambiguously determined. After contact with oxalate solutions of a concentration ≥10 mM, a clear preferential orientation can still be observed; however, the precipitation is somewhat chaotic and irregular aggregates form (Fig. 1c and d). Interestingly, at a high oxalate concentration (100 mM), the crystals forming the calcium oxalate rim appear smaller; also, the oxalate crust covering the unreacted calcite crystal appears more compact, and etch pits are not clearly visible on the substrate surface (compare Fig. 2a, b and c). Furthermore, the gap between the unreacted calcite and the

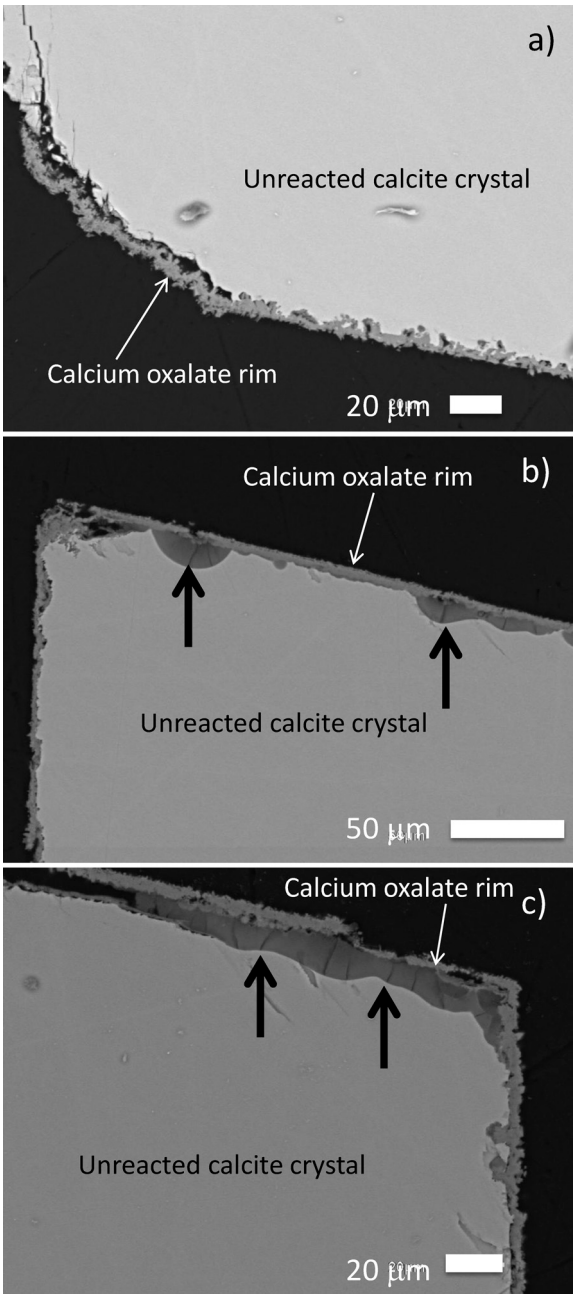

Fig. 3 FESEM backscattered electron images of calcite crystals partially replaced by Ca-oxalate and embedded into epoxy resin blocks before sectioning. Cross-sections after contact with 1 mM oxalate solution (pH 3.0, solution volume, 60 mL) during (a) 24 hours, (b) 120 hours and (c) 168 hours. Note the formation of an oxalate ring with two different textures. Cracks (marked by the thick black arrows) form in the replacement product.

Published on 06 September 2013. Downloaded by Universidad de Granada on 02/12/2013 06:34:40.

calcium oxalate product was not detected. SEM images of cross-sections and surfaces of partially replaced samples show a texture totally different from that of the parent calcite. Partially replaced calcite crystals preserve the morphology (*i.e.* external dimensions and crystallographic characteristics) of the initial crystal fragments, *i.e.* calcium oxalate replaces calcite pseudomorphically. In the cross-section images, two different replacement crusts can be observed. At short reaction time (24 hours, Fig. 3a), a crust *ca.* 5 to 10 μm is formed where individual crystals are clearly differentiated and with visible porosity. This layer is still present after 120 and 168 hours (Fig. 3b and c, respectively) but does not increase in thickness. However, a second rim, which is more compact, not homogenously distributed on the substrate surface and with no visible porosity, forms at these longer contact times. Dissolution of the parent calcite crystal is seen by the formation of deep etch pits on the substrate surface just beneath the newly formed precipitate (see Fig. 2 and 4). Interestingly, most of the empty spaces observed in both reaction rims are related to the formation and widening of cracks. These cracks are commonly visible both within the replacement product and within the non-reacted calcite crystals (Fig. 3 and 4), parallel to the (104) surface of the parent crystal and, to a lesser extent, forming an angle of *ca.* 43° to the calcite cleavage surface. The replacement is initiated at the calcite cleavage surface but also proceeds preferentially along the cracks once they have formed (Fig. 4a and b). This also demonstrates that the observed fractures are not formed as a result of the protocol for sample preparation (*i.e.* polishing). With the progress of the reaction, the replacement product separates from the calcite surface and breaks down into fine particles. This precludes obtaining any quantitative information regarding the kinetics of the reaction from the analysis of the reaction rim thickness. The frailty of the reaction product seems to be the result of both the low coherence of the reaction interface and the presence of fractures. Nevertheless, the calcite–calcium oxalate replacement interface is always coherently retained, and the first thin calcium oxalate rim could be observed in all the studied samples. When a high fluid-to-solid ratio (*ca.* 200 mL solution per 0.030 g of calcite) and long contact times (1 week) were used, the advancement of the reaction and the related fracturing and detachment of the replacing product resulted in the formation of a round remnant core of unreacted calcite (Fig. 4c and d).

In the experiments carried out at pH *ca.* 6.5, the textures are remarkably different (Fig. 5a and b). The overgrowing

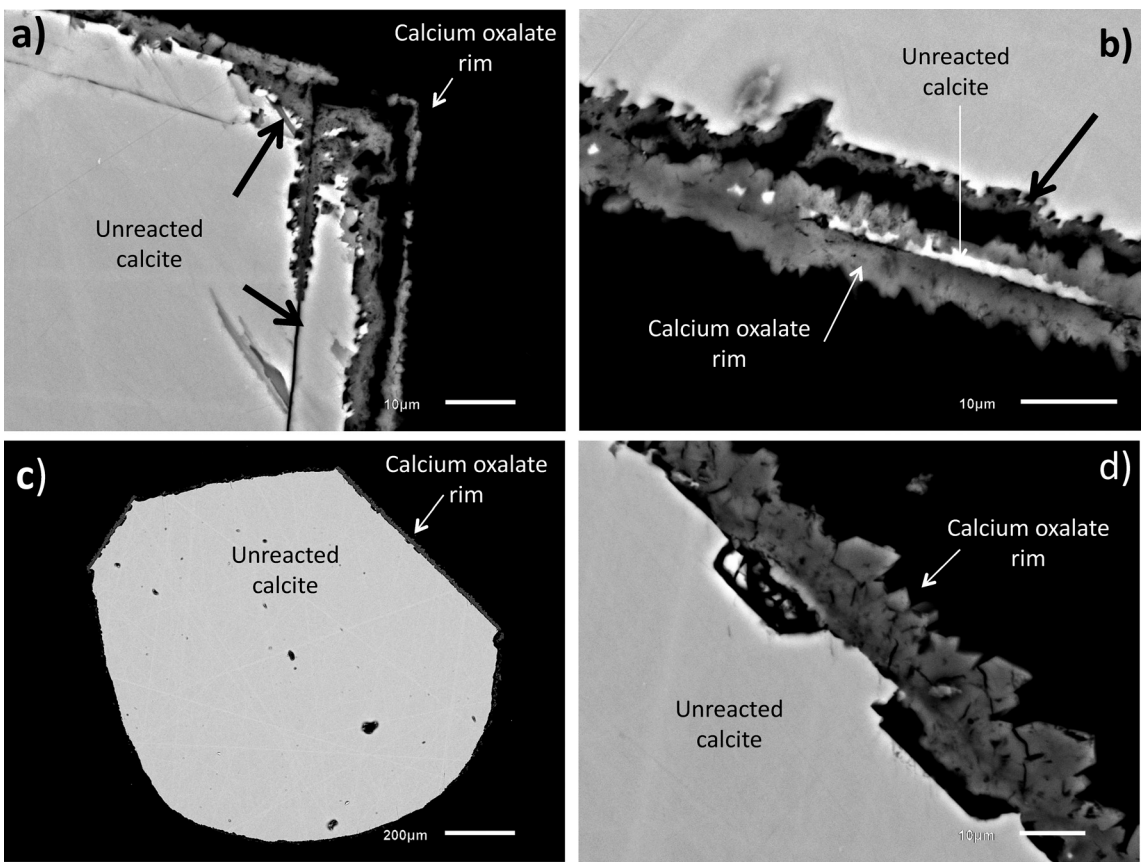

Fig. 4 FESEM backscattered electron images of calcite crystals partially replaced by Ca-oxalate and embedded into epoxy resin blocks before sectioning. (a) Cross-section of a partially replaced crystal after 1 week of contact with 1 mM oxalate solution (pH 3.0, solution volume, 60 mL). Note the preservation of the shape of the original Iceland spar (calcite) fragment. (b) Details of (a), showing the formation of cracks on the calcite substrate and the progression of the reaction from both sides of the detached fragment. (c) Cross-section of a partially replaced crystal after 1 week in contact with 1 mM oxalate solution (pH 3.0, solution volume, 200 mL). Note rounding of the original rhombohedral fragment. (d) Details of (c), showing etch pits on the calcite substrate and cracks in the Ca-oxalate rim, as well as a clear preferred orientation in the Ca-oxalate crystals with respect to the substrate.

 This journal is © The Royal Society of Chemistry 2013

Published on 06 September 2013. Downloaded by Universidad de Granada on 02/12/2013 06:34:40.

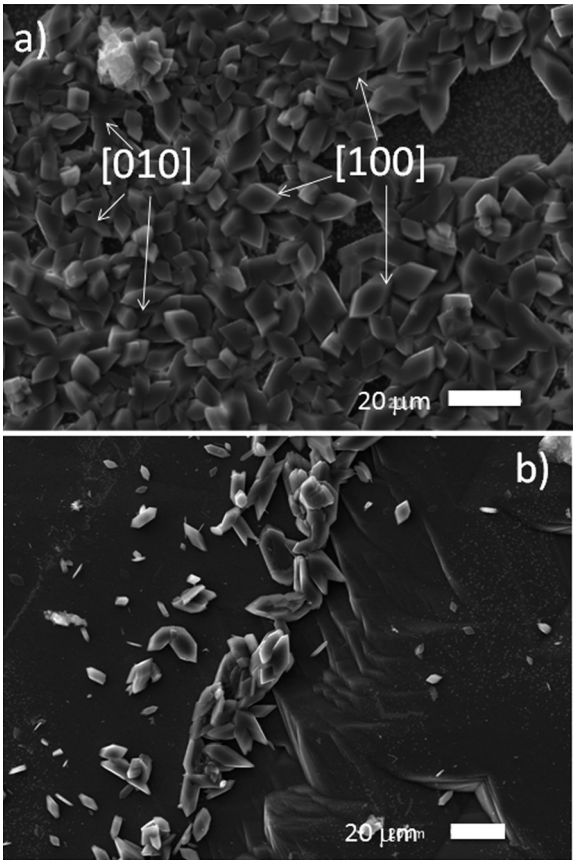

Fig. 5 FESEM secondary electron images of calcite crystals partially replaced by Ca-oxalate. Surfaces of partially replaced crystals after 72 hours of contact with (a) 1 mM oxalate solution, pH 6.5, solution volume, 60 mL, and (b) 0.1 mM oxalate solution, pH 6.5, solution volume, 60 mL.

crystals do not show a clear orientation on the calcite substrate as seen in FESEM observations. The crystal habit of the overgrowing whewellite in this case is predominantly equant, showing {100} and {010} faces parallel to the original calcite surface. Here, the precipitation is somewhat chaotic, commonly with the formation of irregular aggregates, so that a preferential orientation of the replacing crystals is not evident.

(b) Epitaxial orientation of calcium oxalate crystals on calcite surfaces

A 2-dimensional XRD pattern of a partially converted calcite sample after three days of contact with a 1 mM $H_2C_2O_4$ solution (pH 3.1) is shown in Fig. 6. The strong single spots belong to the original calcite crystal, while the Debye–Scherrer rings correspond to the overgrowing whewellite crystals. Notice that, superimposed on the diffraction rings, the intensity is concentrated in arcs indicating that a significant fraction of whewellite crystals have a strong preferential orientation. From the analysis of the pole figures calculated for the main calcite and whewellite reflections (Fig. 7), it can be deduced that whewellite crystals nucleated on the {104} calcite faces with either their {100} or {010} planes parallel to this calcite plane. 2D-XRD analysis showed similar crystallographic orientations at low and high pH values.

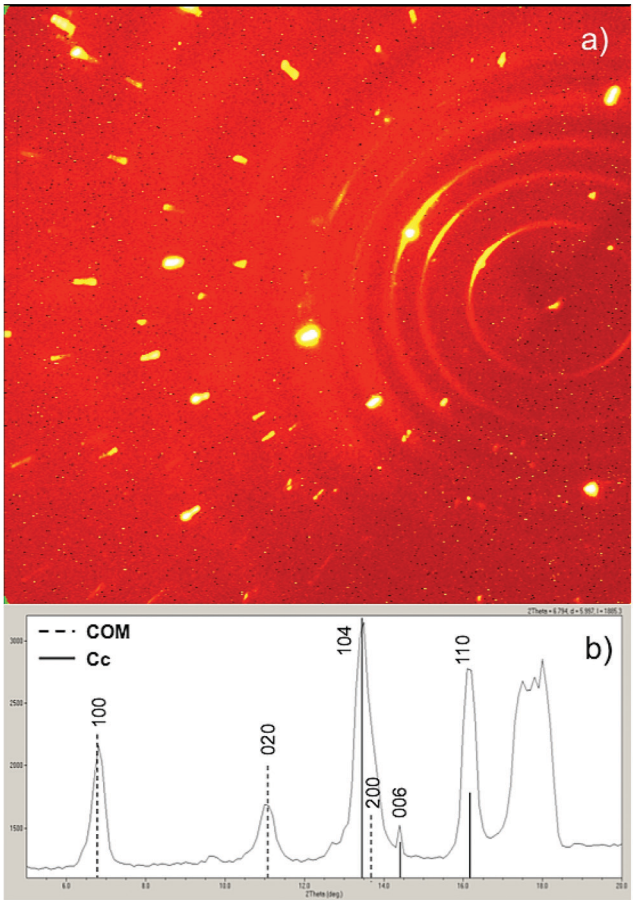

Fig. 6 a) Bidimensional X-ray diffraction (2D-RXD) pattern (phi-rotation scan) from the original crystal (strong single diffraction spots) into whewellite crystals (Debye–Scherrer ring intensities are concentrated in arcs indicating a preferred crystal orientation). b) 2θ scan profile obtained from the radial integration of the 2D-RXD pattern.

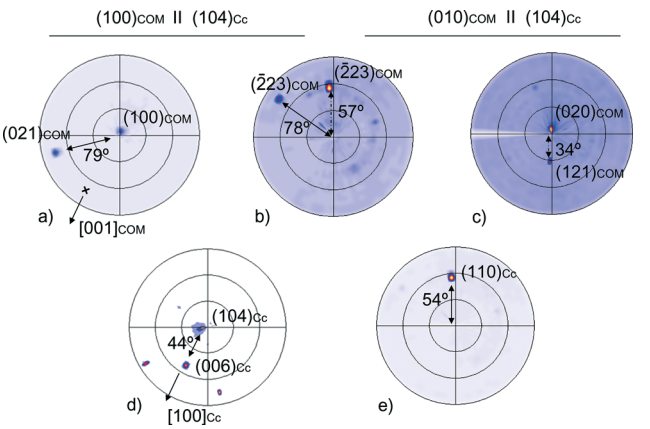

Fig. 7 Pole figures (PF) obtained by 2D-RXD patterns showing the crystallographic orientation relationships between the original calcite crystal and overgrowth whewellite crystals: $(100)_{COM}\|(104)_{Cc}$ and $(010)_{COM}\|(104)_{Cc}$. a) PFs for (100) and (021) whewellite crystals tilted 79°. b) PF for (−223) whewellite crystals displaying two maxima related to (100) and (020) orientations, corresponding to PF centre, tilted 78° and 57°, respectively. c) PFs for (020) and (121) whewellite crystals displaying two maxima related by a tilt of 34°. d) PFs for (104) calcite crystal displaying three maxima tilted 44° from a (006) calcite maximum, distributed according to three-fold symmetry of calcite; d) PF for a (110) calcite crystal showing a defined maximum at a tilt of 54° from the center of the figure, corresponding to the orientation of a (104) calcite crystal.

Published on 06 September 2013. Downloaded by Universidad de Granada on 02/12/2013 06:34:40.

Interestingly, most of the calcite samples showed mechanical twinning, as inferred from the occurrence of duplicated spots, separated by *ca.* 10–20°.[11] In the same way, arcs produced by the oriented whewellite crystals are also duplicated. This fact is further evidence for the strong control exerted by the parent calcite substrate on the orientation of the whewellite crystals. Nevertheless, for simplicity, the orientation relationships between calcite and whewellite were calculated in untwinned calcite specimens. Interestingly, and despite the fact that XRD results show similar orientation relationships in samples replaced under low and high pH conditions, as inferred from SEM observations, the degree of orientation is much higher in the case of samples treated with low pH oxalate-bearing solutions compared to those obtained after reaction of calcite fragments with nearly neutral pH oxalate solutions.

These results are in agreement with AFM observations. Once the oxalate-bearing solution was in contact with the calcite crystal in the AFM fluid cell and after a period where only calcite dissolution was observed (by the nucleation and spreading of rhombohedral etch pits), the nucleation and growth of a new phase was observed. Thus, AFM experiments enabled direct observations of the replacement of calcite by calcium oxalate. The reaction of calcite surfaces with oxalate-bearing solutions followed a pathway of dissolution of the substrate followed by precipitation of thick nuclei or three-dimensional islands of a calcium oxalate phase. Nucleation occurred preferentially on specific sites on the calcite surface, mainly on areas of high step density, over edges with arrow-like shapes formed after dissolution of calcite surfaces upon prolonged contact with oxalate-bearing solutions (Fig. 8). The angular relationships indicate that these step corners are outlined by $\langle \bar{4}41]_{Cc}\rangle$ step edges. This was not observed, however, on initially flat zones, with low step density and wide terraces, where only calcite dissolution by the typical nucleation and widening of etch pits was detected. Calcium oxalate islands exhibited a truncated pyramidal shape. Interpenetration twins were also observed. Measurements performed in AFM images as well as comparison with crystal morphology simulated using SHAPE software indicate that the morphology of whewellite islands is defined by the {010} form, which appears parallel to the (104) plane of calcite. They appear clearly oriented with respect to the calcite [104] surface, with one of their edges parallel to the $\langle \bar{4}41\rangle$ calcite direction.

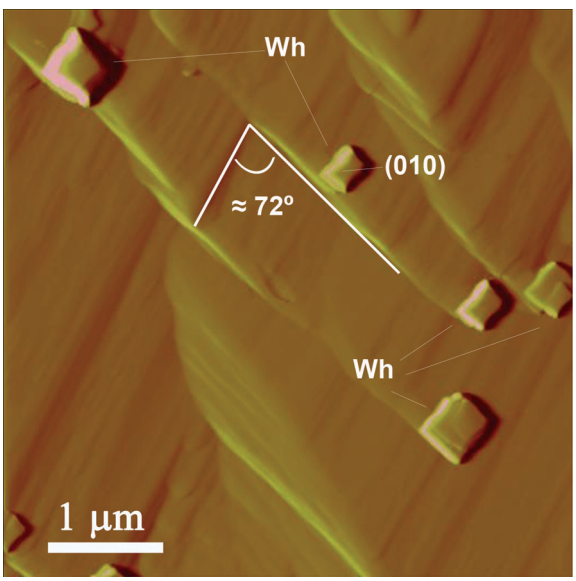

Fig. 8 AFM deflection image showing the epitaxial overgrowth of whewellite on the (104) calcite cleavage surface (Cc = calcite, Wh = whewellite). The initial solution was supersaturated with respect to whewellite (saturation index, 0.17) and undersaturated with respect to calcite.

Discussion

(a) Replacement mechanism

The textural evidence shown in the experimental observations suggests that the $CaCO_3$–CaC_2O_4 transformation is an interface-coupled dissolution–precipitation reaction. As shown by Xia and co-workers,[12] the coupling between dissolution and precipitation processes in such replacement reactions arises from a combination of substrate-assisted nucleation and solution chemistry at the reaction interface. The dissolution of calcite increases the activity of Ca^{2+} in the solution directly at the interface with the reacting solid, thus leading to an increase in the degree of saturation of such a fluid with respect to $CaC_2O_4{\cdot}H_2O$, which promotes its nucleation. This effect is further augmented by the structural matching existing between calcite and whewellite that promotes the nucleation (by decreasing the energy barrier for nucleation) and subsequent epitaxial growth of whewellite on calcite surfaces. The precise epitaxial relationships and structural matching between these phases are detailed in a subsequent section (see Section (d)) below. The fact that whewellite precipitates as thick three-dimensional crystals,not forming continuous layers on the substrate, is typically a consequence of weak adhesion between substrate and product which is in agreement with a "Volmer–Weber" mechanism of epitaxial growth.[13] Calcium and oxalate ions form a continuous network of strong Ca–O bonds both along various directions within the (100) plane and between the (100) layers. This confers a high surface energy to the (100) and (010) planes.[14] For this reason, whewellite does not form continuous layers or thin plates on the calcite surface. Any slight mismatch between the calcite substrate and the overgrowth crystal faces will result in the formation of 3D islands, which tend to grow preferentially perpendicular to the surface (*i.e.* increasing their height), as lateral spreading of these nuclei is energetically unfavourable. This mechanistic interpretation was also confirmed by the *in situ* nanoscale AFM observations.

(b) Kinetic control of the degree of pseudomorphism

The extent of coupling between the dissolution and precipitation in replacement reactions determines the degree of preservation of the parent crystal morphology. Perfect coupling between precipitation and dissolution must occur right at the reaction interface for the crystallographic orientation and

 This journal is © The Royal Society of Chemistry 2013

Published on 06 September 2013. Downloaded by Universidad de Granada on 02/12/2013 06:34:40.

textural features of the parent phase to be preserved in the replacement product.[12] This occurs when the replacement product rapidly nucleates just next to the parent solid dissolution site. As shown by Putnis *et al.*,[4] the dissolution and precipitation process is confined to a fluid boundary layer at the reaction interface, which has a different composition to the fluid in the bulk. According to our results, pH, more than oxalate concentration, is the critical factor controlling this process.

Calcite dissolution rate decreases with increasing pH under conditions far from equilibrium (*i.e.* high undersaturation). At pH < 4, the dissolution is controlled by mass transfer processes, while at pH > 5.5, surface chemical reaction becomes the dominant process.[15] This means that under conditions of low pH, calcite dissolution will be rapid compared to mass transport within the fluid, thus allowing the build-up of high supersaturation with respect to whewellite in the boundary layer close to the crystal surface. This leads to the fast nucleation and subsequent growth of this phase in close proximity to the substrate surface. Furthermore, as mentioned above, the structural similarities existing between calcite and whewellite results in a decrease in the activation energy for whewellite nucleation, contributing to the rapid nucleation and growth of the product phase, whose orientation will be controlled by the underlying structure of the substrate. All in all, fast nucleation right at the dissolution site and substrate-assisted growth of whewellite results in tight coupling between calcite dissolution and whewellite growth. Fast nucleation seems to require concentrations of oxalate above 1 mM (at pH 3) as well; as for lower concentrations, no clear orientation of the whewellite crystals is observed. Therefore, these conditions are optimal to obtain a pseudomorph that precisely preserves the external dimensions and shape of the original calcite crystal during the replacement.

Under conditions close to neutrality, the dissolution rate of calcite is considerably lower, and the rate of calcium supply to the solution becomes slow compared to mass transport within the fluid. Thus, the solution will be uniformly supersaturated with respect to whewellite, and its precipitation will occur not only in close contact with the surface but also at longer distances from the substrate. The situation would be in this case closer to nucleation directly from solution (*i.e.* 3D homogeneous nucleation). Although oriented precipitation may still occur to some extent (as inferred from the 2D-XRD results), the precipitation is somewhat more chaotic and crystals appear randomly distributed, as is clearly observed in the SEM images. The lower whewellite crystal density and more equidimensional morphologies observed at higher pH reflect slower nucleation and growth processes as a result of precipitation in conditions close to equilibrium with respect to whewellite (*i.e.* slightly supersaturated solutions).

Finally, it should be indicated that the whewellite growth rate is also influenced by pH, tending to decrease with decreasing pH.[16] However, all our observations suggest that the effect on whewellite growth kinetics of the high supersaturation reached at the boundary layer due to fast calcite dissolution at low pH overcomes the "negative" pH effect on the whewellite growth rate.

(c) Volume changes during the replacement and reaction-induced fracturing

Assuming that there is no solid solution in the system $CaCO_3$–CaC_2O_4, the relative volume change $\Delta V_{reaction}$ during the replacement of calcite by whewellite is given by Pollock *et al.*:[6]

$$\Delta V_{reaction} = 100 \cdot \left(\frac{n_d}{n_p} \cdot \frac{V_{M,Wh}}{V_{M,Cc}} - 1 \right) \quad (2)$$

where n_d is the number of moles of calcite dissolved, n_p is the number of moles of whewellite precipitated, $V_{M,Cc}$ is the molar volume of calcite and $V_{M,Wh}$ is the molar volume of whewellite. As in the study of Pollock *et al.*,[6] several scenarios can be considered. First, we will assume that the initial crystal reacts partly or completely and both the parent phase and the replacement product are in equilibrium with the bulk solution (case I). The porosity generated can be estimated from the overall number of calcite moles dissolved and oxalate moles precipitated at equilibrium using (eqn (2)). These amounts also depend on the relative solubilities of the solids in the fluid phase, which are ultimately a function of the initial composition of the solution (*i.e.* oxalate concentration) (Table 3). This approach assumes that all of the dissolved calcite will mix with the entire solution, and a solid in equilibrium with this solution will precipitate. In a second scenario, incremental layers of replacement are successively formed in local equilibrium with the bulk solution at the reacting front (case II). To determine the volume changes at the replacement front, infinitesimal small reaction steps must be considered. We consider that in each of these infinitesimal steps, a calcite monolayer (*i.e.* 0.3 nm thick) from a $4 \times 3 \times 1$ mm crystal (2.1×10^{-10} moles) dissolves. For each of these infinitesimal small dissolution–precipitation steps, the local volume change can be calculated. The local volume change neglects all contributions of former dissolution–precipitation steps (Table 3).

Table 3 $\Delta V_{reaction}$ (%) during the replacement of calcite by whewellite calculated considering that both the parent phase and the replacement product are in equilibrium with the entire solution (case I) and that incremental layers of replacement are successively formed in local equilibrium with the bulk solution at the reacting front, as a function of the oxalate concentration

	Case I		
$[C_2O_4^{2-}]$ (mM)	V = 60 mL	V = 250 mL	Case II
0.1	−81.6	−81.6	58.4
0.5	−16.9	−16.9	109.2
1	41.9	60.2	110.6
5	110.3	110.3	111.0
10	110.8	110.4	111.0
50	110.9	110.4	111.0
100	111.9	110.5	111.0

Published on 06 September 2013. Downloaded by Universidad de Granada on 02/12/2013 06:34:40.

These two PHREEQC simulations show that both the overall $\Delta V_{reaction}$ for the replacement of calcite by whewellite (case I) and the $\Delta V_{reaction}$ in the initial step of the reaction (case II) are positive for $[C_2O_4^{2-}] \geq 1$ mM. However, for $[C_2O_4^{2-}] = 0.1$ mM, the overall $\Delta V_{reaction}$ is negative (−81.6%), while $\Delta V_{reaction}$ in the initial step of the reaction is positive (58.4%).

A third case can be considered that is the dissolution of a small amount of solid in a thin layer of fluid. As already indicated above, during the replacement, the dissolution and precipitation processes are confined to a fluid boundary layer at the reaction interface with a different composition to the bulk.[4] Thus, calculations assuming equilibration of the parent crystal with the bulk fluid phase (case I and case II) are an oversimplification. Our simulations consider that the replacement process takes place in a series of small reaction steps. In each of these steps, a calcite monolayer (*i.e.* 0.3 nm thick) from a 4 × 3 × 1 mm crystal (2.1×10^{-10} moles) dissolves in a thin layer of solution of defined thickness (from 100 nm to 1 mm), and a local equilibrium state is reached with respect to the product. Once local equilibrium is reached, the resulting solution at the interface mixes with the bulk (by diffusion within the fluid phase) and a new reaction step begins, with a slightly modified composition of the solution at the interface as a consequence of the previous reaction step and the subsequent mixing with the bulk solution. Thus, our simulations allow a calculation of the relative volume change $\Delta V_{reaction}$ for the elemental steps described above for different initial compositions and layer thickness. Since we are considering a dynamic system whose composition evolves continuously with time and thus the solubility of the replacement product also varies, the porosity will also change within the course of the reaction. However, the initial steps of the replacement are critical, as if $\Delta V_{reaction}$ is positive, the reaction may eventually stop. As can be seen in Fig. 9 and Table 4, $\Delta V_{reaction}$ for the initial step of the reaction is a function of the initial concentration of oxalate solution and the thickness of the boundary layer (and thus, of the hydrodynamic conditions of the system) for the initial elemental step of the replacement reaction. Under static conditions (no flow or stirring of the solution), the thickness of the boundary layer will be certainly higher than 10 μm (according to the data determined by Liu and Dreybrod),[17] and thus, no porosity will be generated for the range of oxalate concentrations tested in this study (0.1 and 100 mM). Note that this last simulation is somehow also a simplification of the reality, as the composition in the diffusion layer is not homogeneous. In any case, it is assumed to be closer to the real process than cases I and II.

Our simulations suggest that under our experimental conditions, $\Delta V_{reaction}$ (calculated considering differences in molar volumes as well as the relative solubilities of the dissolving and precipitating phases in the fluid phase) will be more likely positive, and thus, porosity will not be generated. Consequently, the reaction may eventually stop, as the fluid phase cannot penetrate within the solid phase. Note also that our calculations assume that a monolayer of calcite dissolves and a continuous calcium oxalate surface layer forms over the whole substrate surface. However, this is not what we observed during AFM experiments: discrete, thick 3D whewellite growth islands formed instead. For complete surface passivation to occur (*i.e.* zero porosity of the surface precipitate), the thick 3D islands should merge as they grow, but the calculation of the amount of calcite dissolved at this point should also take into account energetic considerations of the surfaces involved in the process. Also, it has to be considered that the composition of the solution will evolve during the replacement process, thus affecting also the solubility of the different phases and, as a consequence, the resulting

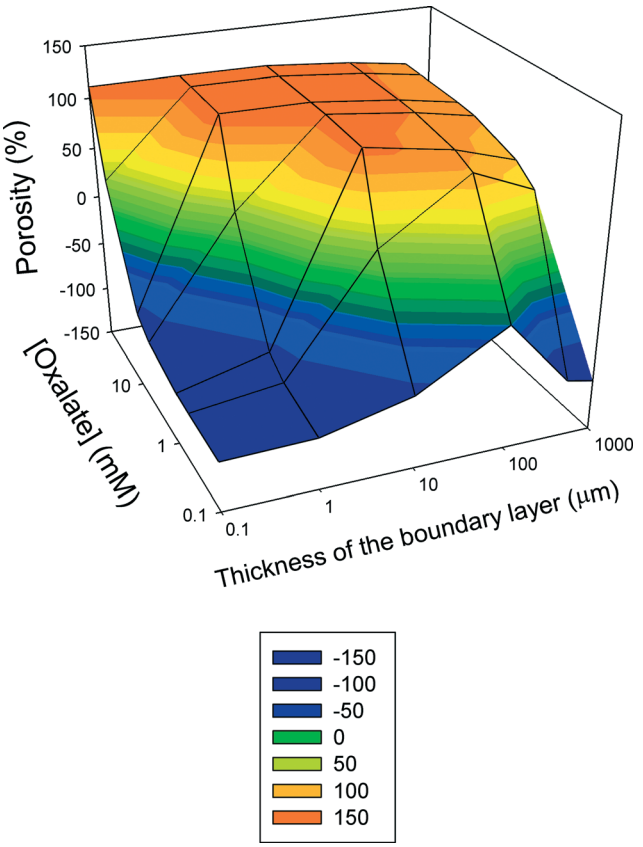

Fig. 9 Porosity in the initial stages of the replacement of calcite by whewellite as a function of the oxalate concentration in solution and the thickness of the boundary layer in contact with the reacting mineral.

Table 4 $\Delta V_{reaction}$ (%) in the initial steps of the replacement of calcite by whewellite, calculated considering the dissolution of a calcite monolayer into a thin layer of fluid, as a function of the oxalate concentration and the thickness of the fluid layer

	Boundary layer thickness (μm)					
$[C_2O_4^{2-}]$ (mM)	0.1	1	10	100	500	1000
0.1	−99.8	−97.5	−76.0	−25.3	−93.8	−99.6
0.5	−98.7	−87.1	26.8	83.5	58.4	−98.5
1	−97.4	−74.2	106.8	92.1	73.6	−74.3
5	−87.0	29.6	109.9	99.7	88.4	−1.8
10	−74.1	110.7	110.0	100.8	90.6	9.2
50	29.7	110.9	110.1	102.1	93.2	22.0
100	111.0	110.9	110.2	102.6	94.2	27.1

 This journal is © The Royal Society of Chemistry 2013

Published on 06 September 2013. Downloaded by Universidad de Granada on 02/12/2013 06:34:40.

porosity. This may well explain the formation of the double rim with the two different textures that would correspond to two different stages of the replacement process characterized by different fluid compositions.

Furthermore, porosity is not the only pathway for the fluid to reach the interface of the unreacted solid. Our observations suggest that fractures form in response to the stresses generated in the replacement rim when there is a positive volume change during the transformation of calcite to whewellite (*i.e.* reaction-induced fracturing). Additionally, cracks can develop when the difference between the lattice parameters of the substrate and the overgrowth is not too high and a coherent substrate–overgrowth interface forms. This leads to the generation of elastic strain as a consequence of stresses produced by the mismatching between the corresponding lattice planes.[18] The elastic energy stored increases the free energy of the system, and thus, stress relaxation may take place, in this case, through the formation of cracks in both the replacement rim and the parent calcite crystal.

These fractures are critical for the progress of the replacement reaction in systems where $\Delta V_{\text{reaction}}$ calculated from molar volumes and relative solubilities is positive. They provide pathways for the solution to reach fresh, unreacted calcite surfaces that rapidly react with the solution in the vicinity. Therefore, fractures allow the advancement of the reaction even in the cases where no porosity is expected from relative molar volume changes and solubility differences between the parent phase and the product. Also, the rate of replacement is expected to be significantly faster than in the hypothetical case of a reaction controlled by diffusion through the porous system of an unfractured replacement rim of whewellite.[19] Nevertheless, the appearance of these cracks makes the product very brittle and friable and thus easily detachable from the substrate. This explains why thick pseudomorphic replacement rims are not observed even in the advanced stages of the replacement. A very similar behaviour has been previously reported for other replacement reactions such as the replacement of leucite by analcime.[19,20] Also, in our experiments, the cracks divide the parent calcite into smaller fragments that detach from the parent crystal and are subsequently replaced by whewellite (Fig. 5b).

(d) Epitaxial relationships between whewellite and calcite

Whewellite (the low-temperature polymorph of calcium oxalate monohydrate) crystallizes in the monoclinic system with the space group $P2_1/c$ and the following parameters: a = 6.290 Å, b = 14.583 Å, c = 10.116 Å, β = 109.46, Z = 8.[21] In its structure, there are two types of oxalate ions. A first set of oxalate ions (OXa) lies nearly parallel to the (100) plane together with all of the Ca^{2+} ions, with C–C bonds running along [010]. A second set (OXb) lies approximately parallel to the (010) plane (C–C bonds nearly along [001]).[22] Calcite crystallizes in the trigonal system with the space group $R\bar{3}c$. A crystal with a rhombohedral crystal structure can also be defined using hexagonal axes. The hexagonal "structural" cell has $a = b$ = 4.990 Å and c = 17.061 Å. In this setting, the calcium cations and carbonate groups occupy alternate layers perpendicular to the c axis. Within any plane, all the carbonate groups point in the same direction, while neighboring planes of carbonate groups have opposite orientations.

The structural misfit (mf) between two PBCs in the calcite and whewellite structure can be calculated using the following equation:[23]

$$\text{mf}(\%) = \frac{2(t_{[uvw]\text{Cc}} - t_{[uvw]\text{COM}})}{t_{[uvw]\text{Cc}} + t_{[uvw]\text{COM}}} \quad (3)$$

where $t_{[uvw]}$ is the repeating period along the $[uvw]$ direction in calcite (Cc) and whewellite (COM). Misfits of −0.05% and 4.26% were found for $[101]_{\text{COM}}$ and $[010]_{\text{Cc}}$ and $[100]_{\text{COM}}$ and $[\bar{4}41]_{\text{Cc}}$, respectively. The angular misfit between these sets of directions is −5.31°. Thus, very good matching exists between (010) whewellite and (104) calcite faces. These misfit values are clearly within the limits required for epitaxial nucleation from the solution. This explains well one of the two sets of orientations revealed by the 2D-XRD results. Similarly, structural similarities were found along whewellite [001] and calcite [010] PBCs (mf = −1.35%) in $(100)_{\text{COM}}$ and $(104)_{\text{Cc}}$ faces, but simultaneous matching along other crystallographic directions in these faces was not found. Nevertheless, good matching was found in the repeating periods perpendicular to $(100)_{\text{COM}}$ and $(104)_{\text{Cc}}$. The correspondence in the repeating period perpendicular to both faces may be another factor promoting the formation of thick crystals that tend to grow perpendicularly to the surface. It is also worth noting that there is a structural compatibility between the symmetry elements of calcite and whewellite parallel to the a- and b-axes of calcite (*e.g.*, [100] and its equivalent [010] directions) which have a 2-fold symmetry and the c-axis of whewellite (also 2-fold symmetry) that allows an extended structural matching in the perpendicular plane. Additionally, there is a simple proportionality between the a parameter of calcite (4.990 Å) and the c parameter of whewellite (10.116 Å) that allows continuity of the crystal structure in the third dimension.

[101], [100] and [001] whewellite PBCs and their corresponding repeating periods are shown in Fig. 10a and b. Water molecules have been omitted for the sake of simplicity. PBC [100] is composed of alternating double links of chelate bonds and single bonds. PBC [101] is just built by chelate bonds, and PBC [001] is composed of one chelate bond, two single bonds and one hydrogen bond. These strong PBCs determine the F-character of the {100} and {040} whewellite forms. The calcite PBC running parallel to the $[\bar{4}41]$ direction is formed by alternating Ca^{2+} and CO_3^{2-} ions, while that running along the [010] direction is formed by either Ca^{2+} or CO_3^{2-} ions (Fig. 10c and d). All in all, this analysis suggests a crystallographic control of the precipitation of whewellite onto calcite, with two possible epitaxial orientations, which were demonstrated in the XRD pole figure

Published on 06 September 2013. Downloaded by Universidad de Granada on 02/12/2013 06:34:40.

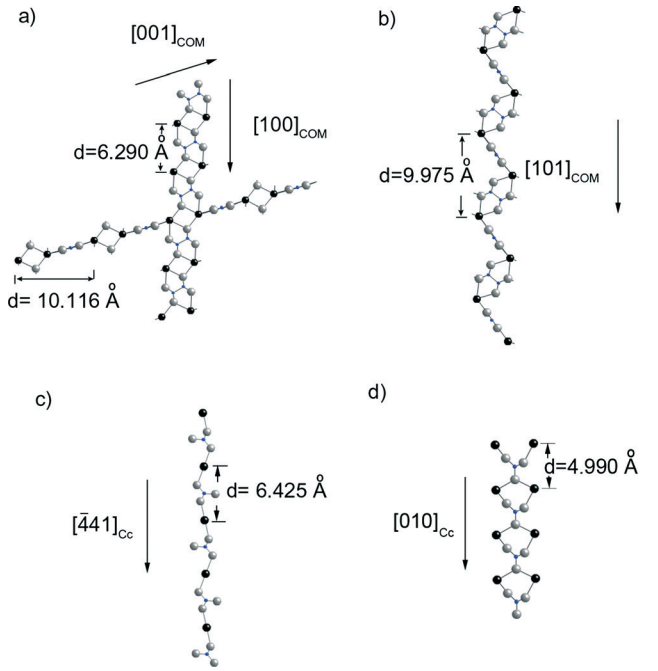

Fig. 10 PBCs in (a) (010) and (b) (100) whewellite faces and in (c, d) (104) calcite face.

analysis of partially replaced calcite crystals: $(010)_{COM}\|(104)_{Cc}$, $[100]_{COM}\|[\bar{4}41]_{Cc}$, and $(100)_{COM}\|(104)_{Cc}$, $[001]_{COM}\|[010]_{Cc}$. Note that these orientations are also in agreement with those most frequently seen in SEM images of whewellite crystals in the replacement rim (see Fig. 1). A SHAPE simulation of the epitaxial relationships is represented in Fig. 11. These relationships are also in agreement with the *in situ* nanoscale AFM observations performed.

Finally, it should be noted that the structural matching between calcite and whewellite does not exist between calcite and other calcium oxalate phases (calcium oxalate dihydrate, COD, and trihydrate, COT). Both COD and COT are more soluble than COM (whewellite). COM precipitation at low supersaturation is facilitated (*i.e.* promoted) by epitaxial nucleation as a result of the good matching between COM and calcite structures, and thus, the solution may not reach supersaturation with respect to COD and COT. This may well explain why only COM (whewellite) was identified in our experiments by 2D-XRD analyses of partially replaced crystals and no other oxalate phases, while their presence is frequently reported in homogeneous precipitation experiments.

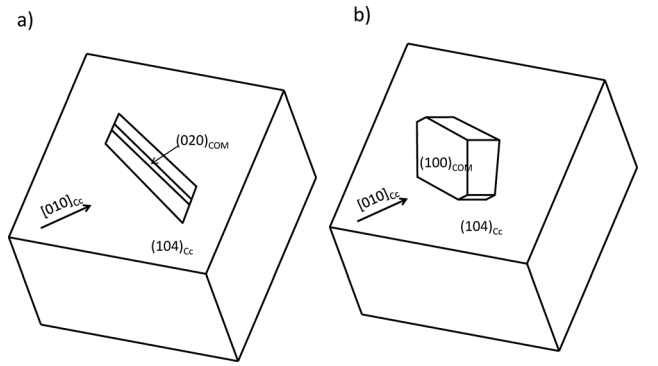

Fig. 11 SHAPE simulation of epitaxial relationships in the calcite–whewellite transformation: (a) $(010)_{COM}\|(104)_{Cc}$, $[100]_{COM}\|[\bar{4}41]_{Cc}$, and (b) $(100)_{COM}\|(104)_{Cc}$, $[001]_{COM}\|[010]_{Cc}$.

Conclusions and implications

The textural evidence shown in this paper demonstrates that the replacement of calcite by whewellite is a coupled dissolution–precipitation process. A pseudomorph may be obtained under conditions of low pH, when calcite dissolution is controlled by mass transfer and spatial coupling between calcite dissolution and calcium oxalate nucleation occurs. The porosity generated as a consequence of the reaction is a function of the hydrodynamic conditions (thickness of the mineral–fluid boundary layer) and the initial composition of the solution (*i.e.* oxalate concentration and pH). Under the experimental conditions tested here, no porosity develops as a consequence of the change in molar volumes or differences in relative solubility of parent and product phases. Nevertheless, the replacement rim product shows a fine powdery texture, as a consequence of the formation of fractures and subsequent rupture of the oxalate layer into smaller fragments in order to accommodate the volume increase. This process represents another pathway for the fluid to reach the surface of the unreacted solid, thus being a factor to consider in the study of porosity development during replacement reactions. However, it prevents the formation of a pseudomorph as the product easily detaches from the surface of the unreacted solid.

The existing structural matching between calcite and whewellite may well result in the promotion of calcium oxalate crystallization by calcite, given that only COM, and no other Ca-oxalate phases, forms in our experiments. This process has important technological implications. Substrate-induced precipitation of calcium oxalate phases may change the availability of free phosphorus as a nutrient for plants in calcareous soils, as the ability of oxalate to readily complex Ca^{2+} ions from the soil solution as well as the precipitation of calcium oxalate phases induced by calcitic supports preferentially captures Ca which is then not available for the precipitation of insoluble Ca-phosphate (apatite) phases. This would result in a marked increase in soluble (and thus, available as nutrient for plant uptake) phosphorous in solution relative to the situation where oxalate is absent.[24] Moreover, this work represents a source of information that may help in the design of effective conservation treatments for ornamental and building calcitic stones based on the *in situ* replacement of the original calcitic substrate by an oxalate protective barrier that, because of its lower solubility and reactivity, may reduce pollution attack to these stones.[2,25–27] Such a process would mimic the natural process of oxalate patina formation taking place when a calcareous stone is exposed to the environment.[28] Finally, calcium carbonate and other calcium-bearing phases (*e.g.* calcium phosphate) are

 This journal is © The Royal Society of Chemistry 2013

Published on 06 September 2013. Downloaded by Universidad de Granada on 02/12/2013 06:34:40.

minerals frequently found in stones that form in biological fluids such as in gallstones as well as salivary, pancreatic and kidney stones. Inhibiting the formation of calcium-bearing phases with a high degree of structural similarity to whewellite might play an important role in the prevention of calcium oxalate stone formation in biological fluids.

Acknowledgements

This research project was funded by the European Commission (grant MRTN-CT-2006-34588), the Spanish Government (grants CGL2011-25906 and MAT2012-37584) and the Junta de Andalucía (research group RNM-179 and project P11-RNM-7550). E. Ruiz-Agudo also acknowledges the receipt of a Ramón y Cajal grant from the Spanish Government (Ministerio de Economia y Competitividad). The research at the University of Münster is supported by the Deutsche Forschungsgemeinschaft (DFG). We would also like to thank the two anonymous reviewers for the revision of the manuscript, as well as their helpful suggestions and comments, which helped substantially to improve the quality of our manuscript.

References

1 S. Geider, B. Dussol, S. Nitsche, S. Veesler, P. Berth'ezène, P. Dupuy, J. P. Astier, R. Boistelle, Y. Berland, J. C. Dagorn and J. M. Verdier, *Calcif. Tissue Int.*, 1996, **59**, 33.
2 M. Del Monte and C. Sabbioni, *Environ. Sci. Technol.*, 1983, **17**, 518.
3 A. Putnis, *Mineral. Mag.*, 2002, **66**, 689.
4 C. V. Putnis, K. Tsukamoto and Y. Nishimura, *Am. Mineral.*, 2005, **90**, 1909.
5 A. Putnis, in *Thermodynamics and Kinetics of Water-Rock Interaction*, ed. E. H. Oelkers and J. Schott, Reviews in Mineralogy & Geochemistry, 2009, 30, p. 87.
6 K. Pollok, C. V. Putnis and A. Putnis, *Am. J. Sci.*, 2011, **311**, 211.
7 A. Hesse and D. Heimbach, *World J. Urol.*, 1999, **17**, 308.
8 A. B. Rodriguez-Navarro, *J. Appl. Crystallogr.*, 2007, **40**, 631.
9 D. L. Parkhurst and C. A. J. Appelo, *U.S. Geological Survey Water-Resources Investigation Report 99-4259*, p. 312.
10 L. Brecevic, D. Skrtic and J. J. Garside, *J. Cryst. Growth*, 1986, **74**, 399–408.
11 J. F. Bell, *Am. Mineral.*, 1941, **26**, 247.
12 F. Xia, J. Brügger, G. Chen, Y. Ngothai, B. O'Neill, A. Putnis and A. Pring, *Geochim. Cosmochim. Acta*, 2009, **73**, 1945.
13 A. A. Chernov, *Modern Crystallography III. Crystal Growth*, Springer-Verlag, Berlin, 1984.
14 S. Guo, M. D. Ward and J. A. Wesson, *Langmuir*, 2002, **18**, 4284.
15 E. Sjöberg and D. T. Rickard, *Chem. Geol.*, 1984, **42**, 119.
16 J. F. Desmars and R. Tawashi, *Biochim. Biophys. Acta, Gen. Subj.*, 1973, **313**, 256.
17 Z. Liu and W. Dreybrod, *Geochim. Cosmochim. Acta*, 1997, **61**, 2879.
18 A. G. Shtukenberg, J. M. Astilleros and A. Putnis, *Surf. Sci.*, 2005, **590**, 212.
19 B. Jamtveit, C. V. Putnis and A. Malthe-Sorenssen, *Contrib. Mineral. Petrol.*, 2009, **157**, 127.
20 C. V. Putnis, T. Geisler, P. Schmid-Beurmann, T. Stephan and C. Giampaolo, *Am. Mineral.*, 2007, **92**, 19.
21 V. Tazzoli and C. Domeneghetti, *Am. Mineral.*, 1980, **65**, 327.
22 A. Millan, *Cryst. Growth Des.*, 2001, **1**, 245.
23 A. J. Pinto, E. Ruiz Agudo, C. V. Putnis, A. Putnis, A. Jiménez and M. Prieto, *Am. Mineral.*, 2010, **95**, 1747.
24 J. L. Jurinak, L. M. Dudley, M. F. Allen and W. G. Knight, *Soil Sci.*, 1986, **142**, 255.
25 M. Del Monte, C. Sabbioni and G. Zappia, *Sci. Total Environ.*, 1987, **67**, 17–39.
26 H. Böke and K. L. Gauri, *Water, Air, Soil Pollut.*, 2003, **142**, 59.
27 E. Hansen, E. Doehne, J. Fidler, J. Larson, B. Martin, M. Matteini, C. Rodriguez-Navarro, E. Sebastián-Pardo, C. Price, A. de Tagle, J. M. Teutonico and N. Weiss, *Rev. Conserv.*, 2003, **4**, 13.
28 B. Doherty, M. Pamplona, R. Selvaggi, C. Miliani, M. Matteini, A. Sgamellotti and B. Brunetti, *Appl. Surf. Sci.*, 2007, **253**, 4477.